Surface & Coatings Technology 205 (2011) 4024–4029

Contents lists available at ScienceDirect

Surface & Coatings Technology

journal homepage: www.elsevier.com/locate/surfcoat

# Influence of the C content on the mechanical and tribological properties of the TiCN coatings deposited by LAFAD technique

Y.H. Cheng [a,*], T. Browne [a], B. Heckerman [a], E.I. Meletis [b]

[a] American Eagle Instruments, Inc., 6575 Butler Creek Rd, Missoula, MT 59808, United States
[b] Department of Materials Science and Engineering, University of Texas at Arlington, Arlington, TX 76019, United States

ARTICLE INFO

*Article history:*
Received 20 October 2010
Accepted in revised form 11 February 2011
Available online 18 February 2011

*Keywords:*
Filtered cathodic arc
TiCN coating
Hardness
Elastic modulus
Wear

ABSTRACT

TiCN coatings with different C content were deposited using a large area filtered arc deposition (LAFAD) technique from Ti targets in a mixture of $N_2$ and $CH_4$ gases. Scanning electron microscopy (SEM), nano-indentation, and pin-on-disc tribometer were used to characterize the cross-sectional microstructure, hardness, modulus, wear rate, and friction coefficient of the TiCN coatings. The increase in the $CH_4$ fraction in the gases leads to a continuous increase in the deposition rate of the TiCN coatings as well as an increase in the defect density in the coatings. Nano-indentation results indicate that with an increase of the C content in the coatings, the hardness and elastic modulus increase to a maximum at a C content of 2.8 at.%, then decreases rapidly, which results from the increase in the defect density in the coatings. Tribological test results show that when tested against $Al_2O_3$ balls, there is no significant change in the friction coefficient (0.78–0.88) of the TiCN coatings with a C content of below 4.6 at.%, but the friction coefficient decreases rapidly to 0.21 with a further increase in the C content to 9.3 at.%. In addition, with increasing C content in the coatings from 0 to 9.3 at.%, the wear rate decreases remarkably from $2.5\times10^{-6}$ $mm^3/Nm$ to $5.3\times10^{-7}$ $mm^3/Nm$. The low friction coefficient and the formation of a transfer layer correspond to the low wear rate for the TiCN coatings with high C content.



## 1. Introduction

Surface engineering of cutting tools and mechanical components by the deposition of hard transition metal nitride and carbide coatings has long been proven an effective way to improve their tribological properties, and therefore, their service life [1–4]. Titanium carbonitride (TiCN) coatings are very interesting coatings that combine the high hardness and low friction coefficient of the TiC phases and the high toughness of the TiN phases [5–9]. These unique properties make TiCN coatings a good solution for the applications requiring high abrasion and wear resistance.

A variety of deposition techniques have been developed to deposit TiCN coatings, which include Chemical Vapor Deposition (CVD) [10], Plasma Enhanced Chemical Vapor Deposition (PECVD) [11], and Physical Vapor Deposition (PVD) techniques. Typically, CVD technique was used to deposit TiCN coatings due to the high adhesion, high hardness, and high crystallinity of the deposited coatings. However, the high deposition temperature (1000 °C) limits the selection of the substrate materials. To reduce the deposition temperature, various PVD techniques, such as magnetron sputtering [12], laser ablation [13], cathodic arc [6], and filtered cathodic arc [14,15], were used to deposit TiCN coatings. Filtered cathodic vacuum arc technology is the most attractive technique used to deposit TiCN coatings due to the high ionization rate, high ion energy, and high deposition rate. Using a Large Area Cathodic Vacuum Arc Deposition (LAFAD) technology, we successfully deposited TiCN coatings with Ti targets at a mixture of $N_2$ and $CH_4$ gases, a temperature of 350 °C, and a pressure of 0.02 Pa [15].

It is well known that the structure and properties of the TiCN coatings are strongly dependent on the C content in the coatings [14,16,18]. We also found that the increase in the C content in the TiCN coatings leads to an increase of the grain size, density of the coating, the Ti–C bonding fraction, and the internal stress. It also leads to a decrease in the TiN bonding fraction and the grain size, as well as a change in the growth orientation from (111) to (220) preferred orientation for the coatings deposited by LAFAD [16]. It is expected that the mechanical and tribological properties of the TiCN coatings deposited by LAFAD will be significantly influenced by the C content in the coatings.

In this paper, TiCN coatings were deposited by LAFAD technique from Ti targets under an atmosphere of a mixture of $N_2$ and $CH_4$ gases. The C content in the coatings was adjusted by changing $CH_4$ fraction in the gases from 0 to 50%. The cross-sectional microstructures of the TiCN coatings were investigated by Scanning Electron Microscopy (SEM). The hardness and tribological properties of the TiCN coatings with different C content were characterized and evaluated using nano-indentation and pin-on-disk tribometer. The influence of the C content in the coatings on the

* Corresponding author at: Medtronic Inc., 6800 Shingle Creek Parkway, MS-H134, Brooklyn Center, MN 55430. Tel.: +763 514 0978.
*E-mail addresses:* yuhang.cheng@medtronic.com, yh_cheng@yahoo.com (Y.H. Cheng).

0257-8972/$ – see front matter © 2011 Elsevier B.V. All rights reserved.
doi:10.1016/j.surfcoat.2011.02.032

deposition rate, cross-sectional microstructure, mechanical properties, and tribological properties of the TiCN coatings was systematically studied.

## 2. Experimental details

A LAFAD-1 surface engineering system was used to deposit TiCN coatings. The detailed description of the deposition system was previously published [17]. Briefly, this system consists of one dual filtered arc source, one rectangular plasma-guide chamber, one deposition chamber, auxiliary anodes, heating system, substrate bias system, and a vacuum system. The dual filtered arc source consists of two primary cathodic arc sources utilizing round Ti targets, which are placed opposite each other on the side walls of the plasma-guide chamber, surrounded by rectangular deflecting coils, and separated by an anodic baffle plate. The deposition temperature was controlled by heating elements and measured by a thermal couple located on top of the deposition chamber. The deposition zone for this system is approximately 500 mm in diameter × 300 mm high. 316 and 17-4 stainless steel coupons were used as substrates for characterizing the mechanical properties, surface morphology, bonding structure and crystalline structure. 440a stainless steel coupons were cut from $\phi$187 mm × 182 mm bars, followed by grinding and polishing to a mirror finish surface with a surface roughness (RMS) of about $1.2 \times 10^{-5}$ mm. The wear testings were conducted on the coatings deposited on 440a stainless steel.

The substrates were ultrasonically cleaned and dried before loading into the deposition chamber. Before deposition, the coupons were subjected to Ar plasma cleaning at a pressure, temperature, bias, and time of 0.08 Pa, 350 °C, −250 V, and 15 min, respectively, followed by the Ti ion sub-implantation at a pressure, bias, and time of 0.02 Pa, 500 V, and 2 min. In order to improve the adhesion of the TiCN coatings, a Ti–TiN gradient layer with a thickness of about 200 nm was deposited onto the coupon surface. A gradient layer was deposited by gradually increasing $N_2$ content in a mixed $N_2$ and Ar atmosphere from 0 to 100%. After the deposition of the compositional gradient bonding layer, TiCN coatings with a thickness of 2.5 μm were deposited. The TiCN coatings were deposited at a temperature of 350 °C, pressure of 0.02 Pa, substrate bias of −40 V. To deposit TiCN coatings with different C content, the $CH_4$ fraction in the mixed $CH_4$ and $N_2$ gases was varied from 0 to 50%. The coatings with a $CH_4$ fraction of 5, 10, 20, 30, and 50% were denoted as TiC5N, TiC10N, TiC20N, TiC30N, and TiC50N, respectively.

The coating thickness was measured using a Calo-tester (CSM). The cross-sectional morphology of the TiCN coatings was observed using a Hitachi S-4700 field emission SEM with an acceleration voltage of 20 kV.

Nano-indentation tests were conducted using a MTS nano Indenter® XP (MTS Systems Corp., Oak Ridge, TN, USA) with a Berkovich diamond tip. Hardness and elastic modulus were measured using the continuous stiffness measurement (CSM) option. Si was used as a standard sample for the initial calibration. The hardness and elastic modulus were obtained from the curves using the Oliver–Pharr method.

Conventional ball-on-disk wear testing was used to characterize the dry friction and wear performance for the as-received and the TiCN coated 440a stainless steel coupons. The tribological tests were performed by using a pin-on-disk wear tester (TRB) from CSM Instruments at a load of 1 N and sliding distance of 300 m. During the test, an $Al_2O_3$ ball with a diameter of 6 mm was used as counter material. The wear loss of different samples was measured by a surface profilometer (Veeco Dektak8) scanning across the wear track. The friction coefficient was determined as a function of sliding distance. Wear morphology of the disk was investigated using SEM. The wear morphology of the $Al_2O_3$ balls was characterized by optical microscopy.

## 3. Results and discussions

In order to investigate the detailed structure of the TiCN coatings through the coating thickness, TiCN coated 440a coupons were sliced using diamond saw and the cross sections of the coupons were grinded,

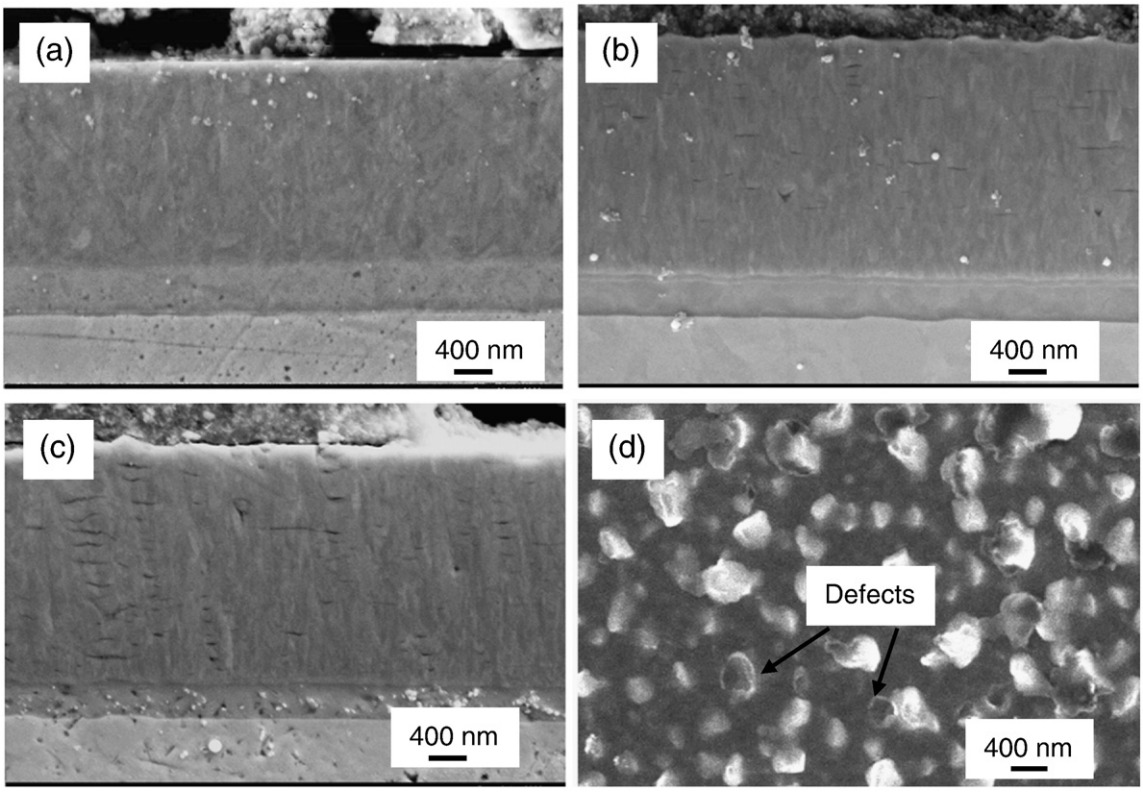


**Fig. 1.** Cross-sectional SEM images of (a) TiN, (b) TiC10N, (c) TiC20N coatings, and (d) plain view SEM image of TiC50N coatings.

polished, and inspected using SEM. Fig. 1 shows the typical cross-sectional SEM images of (a) TiN, (b) TiC10N, and (c) TiC20N coatings. As shown, all coatings consist of two layers, the gradient layer and the TiCN top layer with a thickness of about 0.4 and 2.2 μm, respectively. The top layer of the TiN coatings is very dense and defect free. However, defects or cracks with a length of 200–600 nm parallel to the substrate surface exist in the top 1 μm thick layer of the TiC10N coatings. For the TiC20N coatings, the cracks exist over the entire coating thickness. The formation of the defects or cracks in the coatings may be due to the high internal stress in the TiCN coatings deposited from gases with high $CH_4$ fraction. Fig. 1(d) show s the typical plain view SEM image of the TiC50N coatings. It is interesting to notice that circular defects exist on the coating surface. If we combine Fig. 1(c) and (d), we may conclude that the defects are disk-shaped.

The hardness and modulus of the TiCN coatings on 316 stainless steel substrates were characterized by nano-indentation. The hardness and elastic modulus of 316 steel were also measured to be 6.2 GPa and 213 GPa, respectively, by using the same nanoindenter. Fig. 2 illustrates the hardness and elastic modulus vs. displacement curves for the TiCN coatings deposited from different $CH_4$ fractions. For the pure TiN coatings, the curve exhibits a platform followed by a gradual decrease with increasing displacement of the diamond tip. The hardness corresponding to the platform is about 33 GPa. When 5% of $CH_4$ gas was added into the deposition chamber, the measured hardness and modulus curves show a much higher peak, 43 GPa and 520 GPa, respectively, indicating the high hardness of the TiCN coatings. However, for the coatings deposited with higher $CH_4$ fractions, the measured hardness and modulus curves become more complicated. All the curves exhibit a few shoulder peaks before reaching the main peak. With the increase in the $CH_4$ fraction, the intensity of the main peak decreases and the peak center shifts to the larger displacement of the diamond tip.

The hardness and modulus value in the penetration depth of 5–10% of the coating thickness were averaged and referred to as effective hardness and modulus value of the coatings. Fig. 3 illustrates the effective hardness and modulus of the TiCN as a function of the C content in the coatings. The data in Fig. 3 came from the average of 15 measurements. The details in the method of measuring C content in the coating and the relationship between the CH4 fraction and the C content in the coatings could be found in Ref. [16]. As shown, the effective hardness and modulus increase with increasing C content in the coatings, reaching a maximum of 39.5 GPa at a C content of 2.8 at.%, then decreases linearly with the further increase of C content in the coatings.

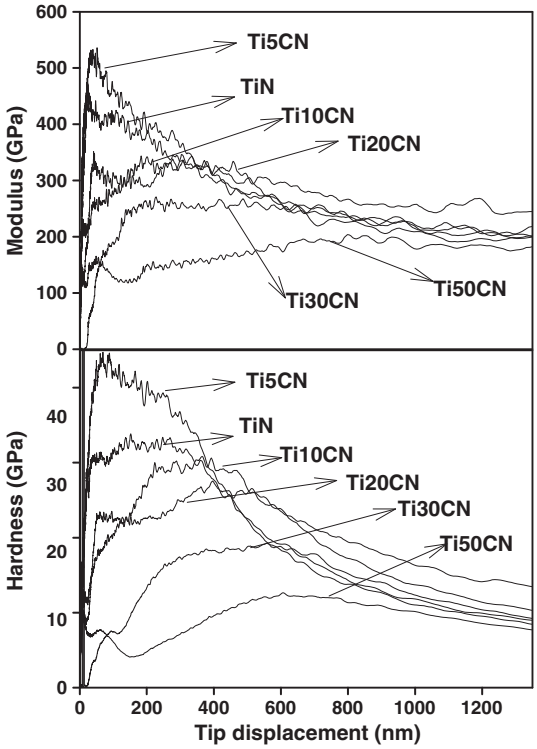


**Fig. 2.** Hardness and elastic modulus of the TiCN coatings deposited from different $CH_4$ fractions.

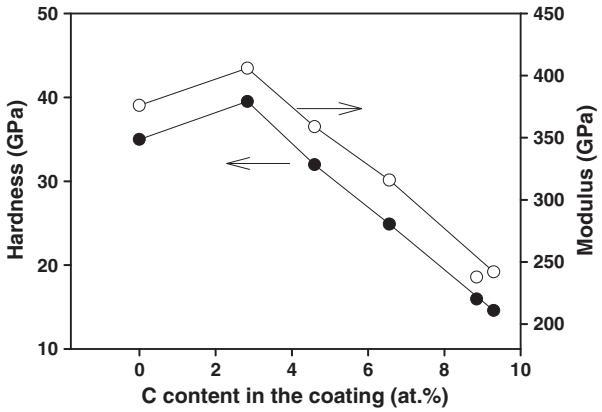


**Fig. 3.** Effective hardness and modulus of the TiCN as a function of the C content in the coatings.

The tribological behavior of TiCN coatings was characterized by a pin-on-disk tribometer. Fig. 4 summarizes the friction coefficient and wear rate of TiCN coatings at the steady state as a function of C content in the coatings. The wear rate was calculated from the surface profilometer measurements. As shown, there is no significant change in the friction coefficient (0.78–0.88) for the TiCN coatings with C content below 4.6 at.% when tested against $Al_2O_3$ balls. However, the friction coefficient decreases rapidly to 0.21 with increasing C content to 9.3 at.%.

The wear rate of the TiCN coatings is strongly dependent on the C content in the coatings. For pure TiN coatings, the wear rate is about $2.5\times10^{-6}$ $mm^3$/Nm. However, after adding 2.8 at.% of C into the coatings, the wear rate reduced 62% to $9.5\times10^{-7}$ $mm^3$/Nm. A further increase of the C content in the coatings to 9.3 at.% leads to a gradual decrease in the wear rate to $5.3\times10^{-7}$ $mm^3$/Nm.

## 4. Discussions

The hardness results, shown in Figs. 2–3, are contrary to the other researchers' reports, which showed a continuous increase in the hardness and modulus with increasing C content in the TiCN coatings

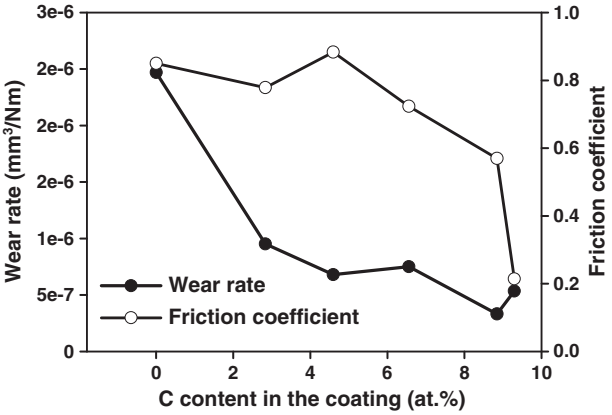


**Fig. 4.** Friction coefficient and wear rate of TiCN coatings against $Al_2O_3$ balls as a function of C content in the coatings.

[14,18]. The cross-sectional SEM results, Fig. 1, show that disk-shaped defects, parallel to the substrate surface, exist in the TiCN coatings deposited from gases with high $CH_4$ fraction. The defect density increases with increasing $CH_4$ fraction. When the nano-indentation tests were conducted on the top of the defect, the diamond tip easily deforms and/or penetrates the layers above the defects, corresponding to low measured hardness and modulus values. For the coatings deposited from gases with high $CH_4$ fraction, the existence of the defects corresponds to the decrease of the measured hardness and modulus value with increasing C content in the coatings. The appearance of the shoulder peaks in the hardness and modulus curves result from the support from the coatings underneath the defects.

The friction behaviors of the coatings are strongly dependent on the coating composition and the formation of transfer layer. Our previous XPS results [16] show that an amorphous carbon exists in the TiCN coatings deposited by LAFAD. The content of the amorphous carbon increases with increasing C content in the coatings. Due to the low shear strength, amorphous carbon is known to exhibit low friction coefficient and can be used to as a solid lubricant. The high amorphous carbon content in the TiCN with high C content corresponds to the low friction coefficient. In addition, the formation of transfer layer, which will be shown in Fig. 7, on the $Al_2O_2$ balls tested against TiCN coatings with high C content also contribute to the low friction coefficient of the TiCN coatings with high C content.

To investigate the wear mechanism of the TiCN coatings against $Al_2O_3$ balls, the surface morphology of the wear track was observed by surface profilometry. Fig. 5 shows the 3-dimensional surface profiles of the wear track for the (a) Ti5CN, (b) Ti20CN, (c) Ti30CN, and (d) Ti50CN coated 440a steel coupons tested with $Al_2O_3$ balls at 1 N and 300 m. On all the TiCN coated surfaces, the wear tracks are very narrow and shallow, indicating excellent wear resistance of the TiCN coatings. Careful inspection of the wear tracks shows very shallow scratches parallel to the sliding direction in the wear track. This indicates an abrasion wear mechanism for the TiCN coatings tested against $Al_2O_3$.

To compare the depth profile of the wear track, the 2 dimensional wear track profiles on the (a) Ti5CN, (b) Ti10CN, (c) Ti20CN, (d) Ti30CN, and (e) Ti50CN coated 440a steel coupons tested against $Al_2O_3$ balls at 1 N for 300 m were plotted in Fig. 6. It is important to point out that the scale ranges of the Y-axis in Fig.6(a) are much larger than that in the other figures due to the very large depth of the wear track. As shown, the wear track on TiN coating surface is much smoother, wider (about 200 μm), and deeper (0.28 μm) when compared with that on TiCN coatings. The maximum depths of the wear track for the Ti5CN, Ti10CN, Ti20CN, Ti30CN, and Ti50CN coatings are 0.16, 0.14, 0.13, 0.13, and 0.13 μm, respectively. This indicates a continuous decrease in the maximum depth of the wear track with increasing C content in the coatings. In addition, a continuous decrease in the width of the wear track with increasing C content in the coatings was also observed.

The formation of a transfer layer on the ball surface significantly affects the wear mechanism and therefore, the wear behavior of the coatings. The wear scar surface on the balls was observed using optical microscopy. Fig. 7 shows the optical images of the wear scar formed on the $Al_2O_3$ balls after the wear test. There is no significant change in the size of the wear scar on the $Al_2O_3$ balls. However, there is a remarkable change in the color of the wear scar. For the coatings with low C content, the wear scar on the $Al_2O_3$ balls exhibits a white color, due to the removal of the ball material. No transfer layer was observed on the wear scar surface except for the area close to the edge of the wear scar. For the coatings with higher C content, the wear scar on the $Al_2O_3$ balls exhibit a grayish color, resulting from the formation of a transfer layer on the scar surface. For the wear scar on the $Al_2O_3$ balls

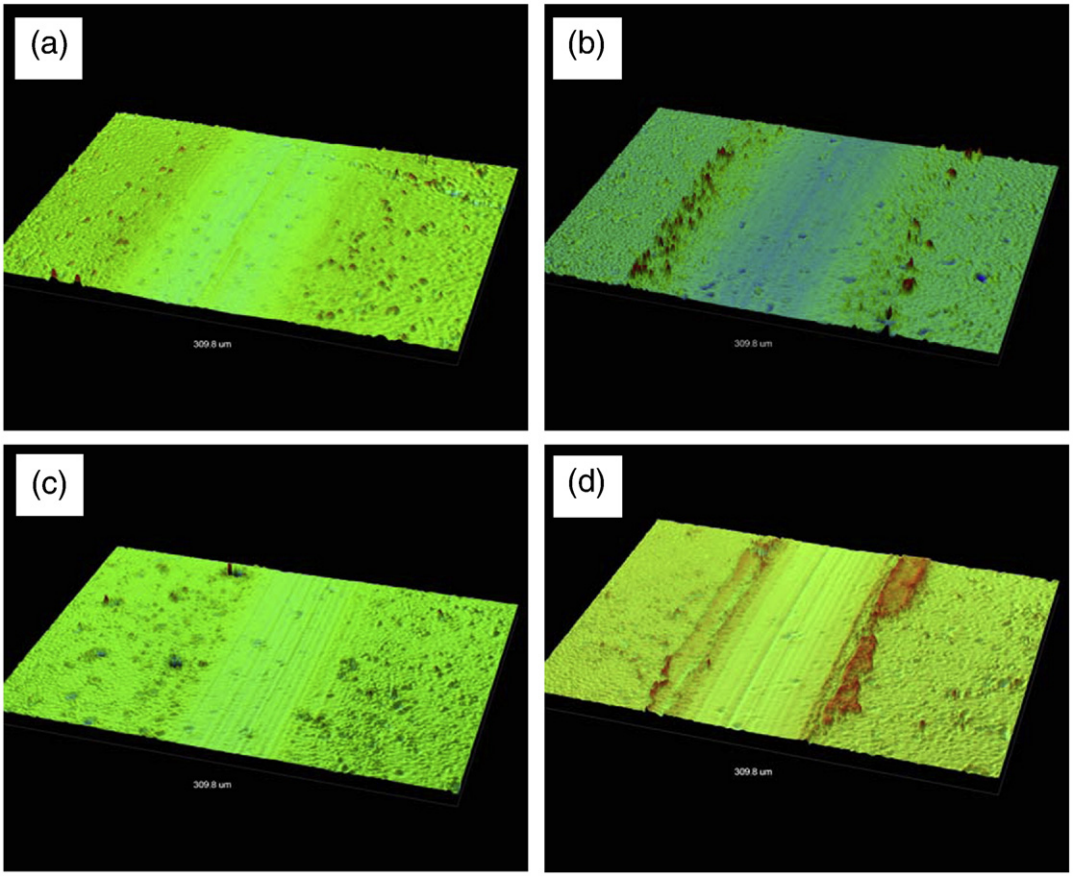


**Fig. 5.** 3D images of the wear track for the (a) Ti5CN, (b) Ti20CN, (c) Ti30CN, and (d) Ti50CN coated 440a coupons.

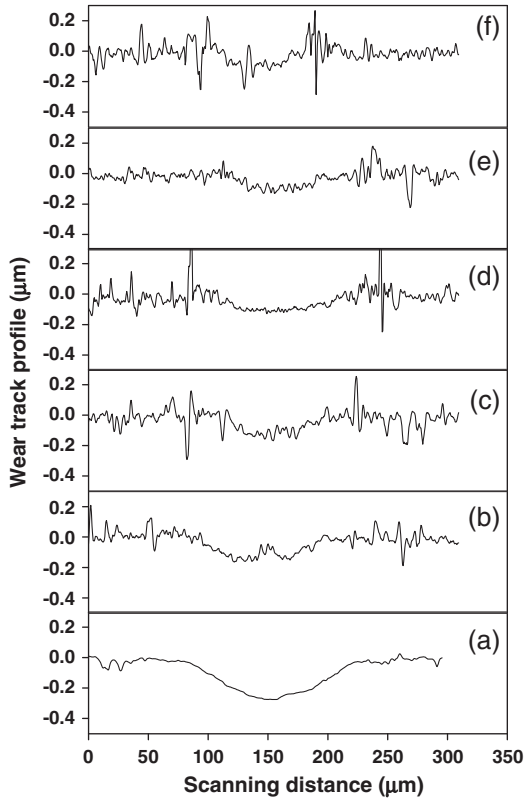


**Fig. 6.** Typical surface profiles of the wear track on the (a) TiN, (b) Ti5CN, (c) Ti10CN, (d) Ti20CN, (e) Ti30CN, and (f) Ti50CN coated 440a steel coupons tested against $Al_2O_3$ balls at 1 N and 300 m.

tested against Ti30CN and Ti50CN coatings, the wear scar surfaces were completely covered by a transfer layer, which significantly affects the wear behavior of the coatings.

The tribological behavior of the coatings is also strongly dependent on the hardness of the coating, friction coefficient, and the formation of a transfer layer on the wear scar surface. For pure TiN coatings, the combination of the relatively low hardness of the coating, large friction coefficient, and absence of the transfer layer on the wear scar surface of the $Al_2O_3$ balls contribute to the high wear rate. When 2.8 at.% of C was added into the coatings, the hardness of the coatings increases significantly, which corresponds to a remarkable decrease in the wear rate. With a further increase in the C content in the coatings, the reduction in the friction coefficient and the formation of a transfer layer on the ball surface cause a gradual decrease in the wear rate.

## 5. Conclusion

TiCN coatings with different C content were deposited by using LAFAD technique from Ti targets under the atmosphere of mixing $N_2$ and $CH_4$ gases. $CH_4$ gas fraction was varied from 0 to 50% to change the C content in the coatings. With increasing C content in the coatings, the hardness and elastic modulus increase to a maximum at a C content of 2.8 at.%, then decreases rapidly. Tribological test results show that there is no significant change in the friction coefficient of the TiCN coatings tested against $Al_2O_3$ balls when the C content in the coatings is below 4.6 at.%, but the further increase in the C content in the coating leads to a rapid decrease in the friction coefficient. It was also found that the increase in the C content in the coatings to 2.8 at.% results in a significant decrease in the wear rate of the TiCN coatings and a further increase in the C content in the coatings results in a slight decrease in the wear rate.

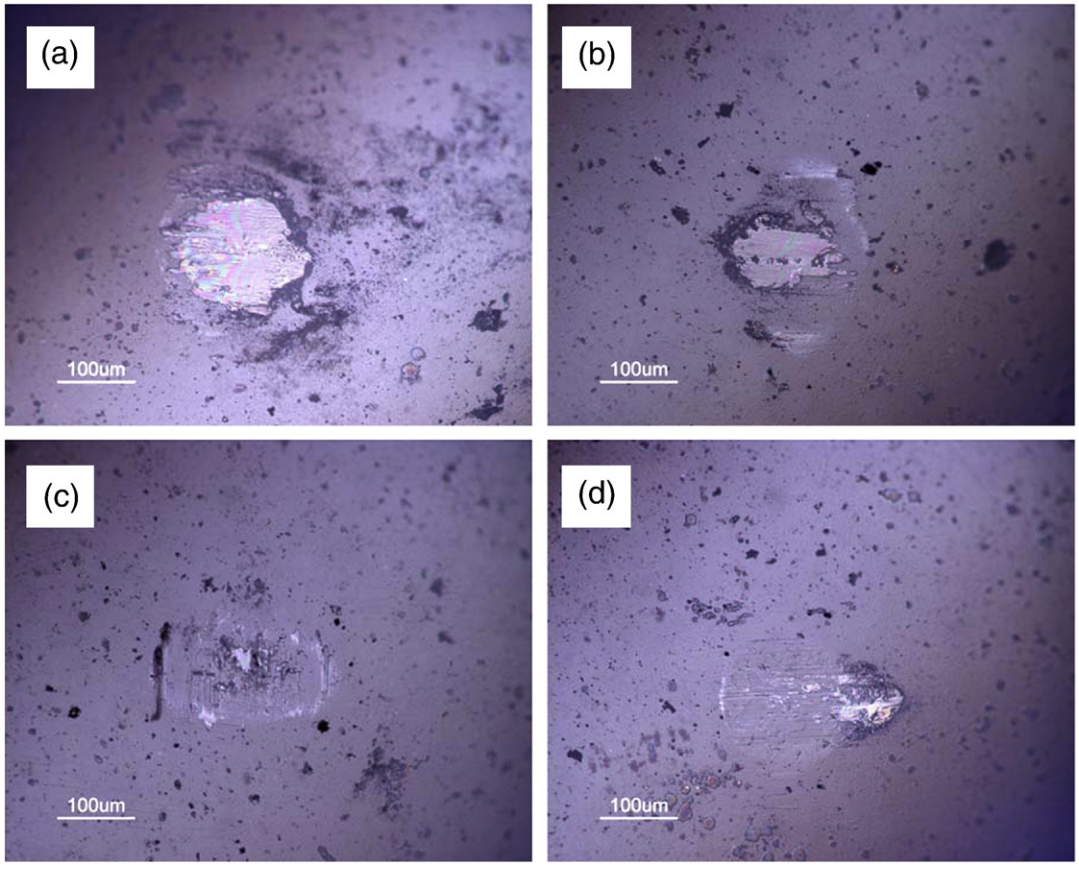


**Fig. 7.** Optical images (20×) of the wear scar on $Al_2O_3$ balls tested against the (a) Ti5CN, (b) Ti10CN, (c) Ti30CN, and (d) Ti50CN coated 440a steel coupons tested at 1 N for 300 m.

## Acknowledgments

The authors would like to express gratitude for the support of The United States Army Telemedicine and Advanced Technology Research Center (TATRC), U.S. Army Medical Research & Material Command under contract number W81XWH-08-2-0023.

## References

[1] P.Eh. Hovsepian, A.P. Ehiasarian, A. Deeming, C. Schimpf, Vaccum 82 (2008) 1312.
[2] S.H. Yao, Y.L. Su, W.H. Kao, K.W. Cheng, Surf. Eng. 21 (2005) 307.
[3] D. Gorscak, P. Panjan, M. Cekada, L. Curkovic, Surf. Eng. 23 (2007) 177.
[4] J. Gerth, M. Larsson, U. Wiklund, F. Riddar, S. Hogmark, Wear 266 (2009) 444.
[5] O. Knotek, F. Loffler, G. Kramer, Surf. Coat. Technol. 61 (1993) 320.
[6] Y.Y. Guu, J.F. Lin, Wear 210 (1997) 245.
[7] J.H. Hsieh, A.L.K. Tan, X.T. Zeng, Surf. Coat. Technol. 201 (2006) 4094.
[8] G. Baravian, G. Sultan, E. Damond, H. Detour, Surf. Coat. Technol. 76/77 (1995) 687.
[9] E. Gergmann, H. Kaufmann, R. Schmid, J. Vogel, Surf. Coat. Technol. 42 (1990) 237.
[10] K. Narasimhan, S.P. Boppana, D.G. Bhat, Wear 188 (1995) 123.
[11] H.L. Wang, J.L. He, M.H. Hon, Wear 169 (1993) 195.
[12] L.C. Agudelo, R. Ospina, H.A. Castillo, A. Devia, Phys. Scr. T. 131 (2008) 014006.
[13] J.M. Lackner, W. Waldhauser, R. Ebner, Surf. Coat. Technol. 188–189 (2004) 519.
[14] S.W. Huang, M.W. Ng, M. Samandi, M. Brandt, Wear 252 (2002) 566.
[15] Y.H. Cheng, T. Browne, and B. Heckerman, J. Vac. Sci. Technol. A, submitted.
[16] Y.H. Cheng, T. Browne, B. Heckerman, Vacuum 85 (2010) 89.
[17] Y.H. Cheng, T. Browne, B. Heckman, J.C. Jiang, E.I. Meletis, C. Bowman, V. Gorokhovsky, J. Appl. Phys. 104 (2008) 093502.
[18] J. Deng, M. Braun, I. Gudowska, J. Vac. Sci. Technol. A 12 (1994) 733.